haematologica
Journal of the Ferrata Storti Foundation

Metabolic plasticity under chronic acidotic stress promotes biphasic adaptive resistance and defines a clinically relevant biomarker signature in multiple myeloma

by Hua-Ling Chen, Pei-Chu Tsai, Sheng-Chieh Lin, Fang-Yu Tsai, Shih Sheng Jiang, Chieh-Lin Jerry Teng and Wun-Shaing Wayne Chang

Received: February 13, 2026.
Accepted: June 8, 2026.

Citation: Hua-Ling Chen, Pei-Chu Tsai, Sheng-Chieh Lin, Fang-Yu Tsai, Shih Sheng Jiang, Chieh-Lin Jerry Teng and Wun-Shaing Wayne Chang. Metabolic plasticity under chronic acidotic stress promotes biphasic adaptive resistance and defines a clinically relevant biomarker signature in multiple myeloma. Haematologica. 2026 June 18. doi: 10.3324/haematol.2026.300533 [Epub ahead of print]

Metabolic plasticity under chronic acidotic stress promotes biphasic adaptive resistance and defines a clinically relevant biomarker signature in multiple myeloma

Hua-Ling Chen,[1] Pei-Chu Tsai,[1] Sheng-Chieh Lin,[1] Fang-Yu Tsai,[1] Shih Sheng Jiang,[1] Chieh-Lin Jerry Teng[2,3] and Wun-Shaing Wayne Chang[1]

[1]National Institute of Cancer Research, National Health Research Institutes, Taiwan; [2]Division of Hematology/Medical Oncology, Department of Medicine, Taichung Veterans General Hospital, Taiwan; [3]Department of Post-Baccalaureate Medicine, College of Medicine, National Chung Hsing University, Taiwan

Correspondence:

W.S.W. CHANG - wayne@nhri.edu.tw; C.L.J. TENG - drteng@vghtc.gov.tw

Disclosures

No conflicts of interest to disclose.

Contributions

HLC designed and performed the majority of experiments. PCT contributed to cell preparation, Western blotting, and bioinformatic analysis. SCL conducted electron microscopy and quantified mitochondrial morphology. FYT and SSJ supervised and interpreted microarray data. CLJT and WSWC contributed to study conceptualization,

methodology, data interpretation, and manuscript writing and revision. All authors read and approved the final manuscript.

Acknowledgements

We thank the Core Instrument Center, including the Cell Sorter Core Lab and Microarray Core Lab, of the National Health Research Institutes (NHRI) for excellent technical support. We are grateful to Dr Chung-Shi Yang and Ms Hsin-Ying Huang (NHRI), as well as Dr Po-Yen Lin and Ms Dia-Nan Lin at Academia Sinica, for kind assistance with transmission electron microscopy. We also acknowledge Drs Hui-Ju Ch'ang, Shine-Gwo Shiah, Shuang-En Chuang, and Hsin-Ling Hsu (NHRI) for providing primary antibodies (CDK2, CCNE2, PDK1, and PKM2) and HRP-conjugated secondary antibodies. Finally, we thank Ms Jia-Rong Tsai of Taichung Veterans General Hospital for administrative support throughout this project. The authors used a large language model (ChatGPT, OpenAI, San Francisco, CA, USA) to assist with language editing and stylistic improvement. All scientific content, data interpretation, and conclusions were generated and verified solely by the authors, who take full responsibility for the integrity and accuracy of the work.

Funding

This work was supported by National Health Research Institutes (CA-112-SP-15/CA-113-SP-05/CA-114-SP-06/CA-113-PP-15/CA-114-PP-15), Taichung Veterans General Hospital (112003/113003/114006), and National Science and Technology Council (112-2314-B-400-011-MY2/114-2314-B-400-017-MY2/114-2740-B-400-005), Taiwan.

Data-sharing statement

Original microarray data used in this study were deposited in Gene Expression Omnibus (GEO) under accession number GSE314522. The authors declare that all the datasets supporting the conclusions of this article are included within the article and its additional files, or are available from the corresponding author (WSWC) upon request.

(Main text: 1,487 words; excluding the title page, figure legends, disclosures, and references)

Multiple myeloma (MM) typically develops over years through the abnormal transformation and asymptomatic expansion of clonal plasma cells.[1] This process is influenced by the bone marrow microenvironment, where chronic extracellular acidosis—arising from exacerbated aerobic glycolysis and compromised vascularization—is a substantial but under-characterized stressor.[2,3] Such microenvironmental acidification has recently emerged as a notable oncogenic factor in solid cancers,[4,5] yet research into hematologic malignancies is restricted to acute, short-term responses.[6,7] In this study, we investigated the long-term consequences of acidic extracellular pH (pH*e*) to reflect the sustained acidotic stress of the marrow niche. We aimed to clarify how MM cells tolerate and adapt to prolonged acidosis and to identify a core adaptive gene signature that correlates with clinical progression and poor prognosis.

To distinguish transient stress from long-term adaptation, we established experimental models (Figure 1A) using human myeloma LP-1 (discovery model; Figure 1) and NCI-H929 (validation model; Online Supplementary Figure S1) cells, both t(4;14)-positive, chronically

exposed to pH*e* 6.8 to mimic the acidity frequently found in the pathological marrow niche.[6,8] To ensure precision and avoid metabolic artifacts associated with lactic acid titration, we employed a rigorous HCl-based protocol to stabilize the target pH*e*,[9] thereby preventing confounding effects on nutrient bioavailability often induced by organic acids. Cells were propagated for short-term (*S.A.*, 2–4 weeks), mid-term (*M.A.*, 4–5 months), or long-term (*L.A.*, 8–10 months) durations. This longitudinal approach captured a slow, reversible adaptive trajectory typically overlooked by conventional acute-exposure models. All subsequent experimental procedures complied with institutional guidelines and national ethical regulations.

Upon initial acidic exposure, both cell lines exhibited decreased proliferation and increased apoptosis (*S.A.* vs *Ctrl*; Figures 1B–C; Online Supplementary Figures S1A–B). Daily monitoring identified a 72-to-96-hour window where apoptosis peaked before survivors acclimated (Online Supplementary Figure S2A). Growth suppression correlated with G1-phase arrest and downregulation of essential cell cycle regulators,[10] including CDK1, CDK2, CCNB1, and CCNE2 (Figure 1C; Online Supplementary Figures S1B & S2A–C). These findings demonstrate that acidosis is fundamentally toxic before it becomes permissive. Nonetheless, the inhibitory effect was transient; continued exposure resulted in a gradual recovery of proliferative capacity and a return of apoptosis rates toward baseline levels (*M.A.* and *L.A.* vs *Ctrl*; Figures 1B–C; Online Supplementary Figures S1A–B). This biphasic trajectory was characterized by the restoration of cell cycle-associated protein expression and proliferative activity in acid-acclimated cells (Figure 1C; Online Supplementary Figure S1B), suggesting a coordinated adaptive program that eventually supersedes initial cytotoxicity.

To determine how acidosis influences MM bioenergetics, we assessed oxygen

consumption rate (OCR) and extracellular acidification rate (ECAR). As depicted in Figure 1D and Online Supplementary Figures S1C & S2D, early exposure markedly suppressed mitochondrial respiration and glycolytic output (*S.A.* vs *Ctrl*). In the chronic adaptive phase, however, OCR/ECAR values rose substantially relative to the acute response (*L.A.* vs *S.A.*), indicating a durable metabolic reorganization and bioenergetic rebound. Although the extent of recovery varied, each cell line reached a stable energetic state sustaining prolonged growth in an acidic milieu. This restoration was complemented by augmented glucose uptake and elevated expression of metabolic enzymes,[11] including SLC2A1, PFKP, PKM2, and LDH (Figure 1D; Online Supplementary Figures S1C & S2E).

Ultrastructurally, this functional recovery was also evident. Early acidosis induced elongated mitochondria with disrupted cristae, indicating structural stress (Figure 1E; Online Supplementary Figure S1D). Yet with prolonged exposure, mitochondria gradually resumed normal ovoid morphology with orderly cristae. To quantify these alterations, we performed morphometric analyses of mitochondrial shape descriptors—circularity, aspect ratio, roundness, and solidity—metrics describing organelle elongation and contour regularity.[12] Descriptor values underwent notable shifts following early acid exposure but returned toward baseline distributions in adapted cells (Figure 1E; Online Supplementary Figure S1D). This phenomenon mirrors stress-induced mitochondrial hyperfusion (SIMH) observed in solid tumors,[13] which preserves ATP production under adverse conditions. Overall, our findings suggest that acute acidotic stress elicits a conserved response in MM cells with marked mitochondrial and metabolic perturbation. With chronic exposure, cells engage an organized adaptive response that abrogates these changes and promotes fitness. This trajectory supports a model in which extracellular acidosis initially imposes a strong inhibitory burden but ultimately orchestrates the metabolic and structural reprogramming

that underlies survival and disease aggressiveness.

This adaptation converges with plasma cell biology. Long-lived plasma cells (LLPCs) reside in specialized marrow niches and require high metabolic robustness to extend antibody production for decades.[14,15] Given that MM involves terminally differentiated plasma cells, it likely co-opts these latent survival strategies. The late-stage, acid-acclimated state characterized here mimics LLPC durability, complemented by mitochondrial functional recovery. Consequently, chronic acidosis operates as an evolutionary sculptor, favoring subpopulations with high mitochondrial resilience and metabolic flexibility, thereby stabilizing LLPC-like survival modules within the bone marrow ecosystem.

To define the molecular landscape of MM cell adaptation to chronic extracellular acidity, we conducted global transcriptomic profiling using Affymetrix microarrays. Pathway enrichment analysis identified hallmark gene sets and canonical pathways modulated during the transition from acute stress to stable adaptation (Figures 2A–B). In particular, pathways governing cell-cycle progression and DNA replication (e.g., E2F targets, G2/M checkpoint) were strongly suppressed during the early stress response but became increasingly enriched as cells reached the long-term (*L.A.*) phenotype (Figures 2A–B). The robust reactivation of these programs in *L.A.* cells indicates the re-establishment of a metabolic steady-state sufficient to support DNA replication, distinguishing chronic adaptation from the transient growth arrest during acute stress. Beyond proliferative recovery, chronic acidosis activated signaling networks involved in tumor progression, such as TGF-β and IL6/JAK/STAT3 pathways. Hierarchical clustering of leading-edge genes revealed a coordinated shift in transcripts linked to survival signaling and metabolic control (Figure 2C), suggesting that prolonged stress drives a dynamic reprogramming toward sustainable malignant adaptation. This molecular landscape remains plastic, as “switch-back” experiments returning *L.A.* cells

to pH*e* 7.4 induced transcriptomic reversibility of representative markers (data not shown), further distinguishing chronic adaptation from fixed clonal selection.

By intersecting transcriptomic profiles of short-term (*S.A. vs Ctrl*; 3,349 probes) and long-term acidification (*L.A. vs Ctrl*; 2,382 probes), as well as the transition between them (*L.A. vs S.A.*; 4,184 probes), we identified a core set of 106 protein-coding genes (represented by 178 probes) consistently modulated across all three contrasts (Figure 3A; Online Supplementary Tables S1A–B). These core transcripts exhibited a highly coherent expression pattern across adaptive stages (Figures 3B–C). Whereas upregulated genes primarily involved mitogenic and cell cycle signaling (e.g., *ANLN*, *CEP55, E2F2*) and metabolic-mitochondrial adaptation (e.g., *ELOVL6*, *PANK1*, *SLC25A53*), the downregulated markers (e.g., *ESR2*, *SLAMF7*) were associated with the suppression of pro-apoptotic and immune-modulatory pathways.

We subsequently filtered this core set using the MMRF-CoMMpass dataset to isolate clinical drivers (Online Supplementary Tables S1A–B). As anticipated, the vast majority of excluded background transcripts showed no significant prognostic relationship (OS.$p > 0.05$), suggesting a highly specific molecular transition under persistent acidic stress rather than a generic cell-stress response. The resulting 11-gene signature, comprising seven long-term acidity-upregulated genes (*E2F2*, *ANLN*, *FAT1*, *CENPI*, *IGFBP7*, *ELOVL6*, *SLC25A53*) and four long-term acidity-downregulated markers (*SLAMF7*, *ESR2*, *GPR160*, *ANKRD36BP2*), reliably predicted overall survival (Figures 3D–E, left panels). To enhance prognostic power, we calculated a composite acidotic adaptive score based on the mean expression of these gene sets. Patients with high mean expression of the seven acidity-upregulated genes exhibited markedly inferior survival ($p = 6 \times 10^{-7}$; Figure 3D, middle panel); conversely, those with low mean expression of the four acidity-downregulated genes demonstrated a comparable

survival disadvantage ($p = 2 \times 10^{-6}$; Figure 3E, middle panel). These adaptive scores closely correlated with clinical stages I–III (Figures 3D–E, right panels). The signature thus uncovers unique microenvironmental drivers of progression that are functionally distinct from proliferation indices or structural genomic aberrations used in established models.

To further validate these clinical drivers across progressive disease evolution, we analyzed independent datasets (GSE6477 and GSE80608). While *SLC25A53* lacked probe representation on these microarray platforms, the remaining ten signature biomarkers tracked progressively from normal plasma cells through MGUS and SMM to overt MM (Online Supplementary Figure S2F). Finally, a Pearson correlation matrix (Figure 3F) confirmed that the upregulated genes exhibited strong positive correlations with one another but significant negative correlations with the downregulated markers, identifying a coordinated molecular module driven by chronic acidotic stress.

In summary, our study demonstrates that chronic acidosis acts as a potent selective force driving MM cell adaptation. We describe a slow, stepwise evolution from acute toxicity to metabolic flexibility and mitochondrial resilience, accompanied by a validated acid-adaptive gene signature. Although prospective validation in larger cohorts and a broader cell line panel remains essential, this signature offers potential as a biomarker of microenvironmental rewiring and a target for focused interference with acidosis-driven progression. These data elucidate the limitations of risk stratification schemes that rely almost exclusively on genomic characteristics while neglecting dynamic microenvironmental forces. Fundamentally, our work supports a view of MM as an evolving ecosystem in which malignant plasma cells gradually acquire tolerance under persistent extracellular acidosis—a dynamic process reflected in the protracted and relapsing clinical history of this disease.

References

1. Maura F, Bergsagel PL. Molecular pathogenesis of multiple myeloma: clinical implications. Hematol Oncol Clin North Am. 2024;38(2):267-279.
2. Kühnel A, Blau O, Nogai KA, Blau IW. The Warburg effect in multiple myeloma and its microenvironment. Med Res Arch. 2017;5(9):1-16.
3. Gastelum G, Veena M, Lyons K, et al. Can targeting hypoxia-mediated acidification of the bone marrow microenvironment kill myeloma tumor cells? Front Oncol. 2021;11:703878.
4. Corbet C, Feron O. Tumour acidosis: from the passenger to the driver's seat. Nat Rev Cancer. 2017;17(10):577-593.
5. Wu TC, Liao CY, Lu WC, et al. Identification of distinct slow mode of reversible adaptation of pancreatic ductal adenocarcinoma to the prolonged acidic pH microenvironment. J Exp Clin Cancer Res. 2022;41(1):137.
6. Watanabe K, Bat-Erdene A, Tenshin H, et al. Reveromycin A, a novel acid-seeking agent, ameliorates bone destruction and tumor growth in multiple myeloma. Haematologica. 2021;106(4):1172-1177.
7. Amachi R, Hiasa M, Teramachi J, et al. A vicious cycle between acid sensing and survival signaling in myeloma cells: acid-induced epigenetic alteration. Oncotarget. 2016;7(43):70447-70461.
8. Lombardi AF, Wong JH, High R, et al. AcidoCEST MRI evaluates the bone microenvironment in multiple myeloma. Mol Imaging Biol. 2021;23(6):865-873.
9. Michl J, Park KC, Swietach P. Evidence-based guidelines for controlling pH in mammalian live-cell culture systems. Commun Biol. 2019;2:144.

10. Pellarin I, Dall'Acqua A, Favero A, et al. Cyclin-dependent protein kinases and cell cycle regulation in biology and disease. Sig Transduct Target Ther. 2025;10:11.
11. Martell E, Kuzmychova H, Senthil H, et al. Compensatory cross-talk between autophagy and glycolysis regulates senescence and stemness in heterogeneous glioblastoma tumor subpopulations. Acta Neuropathol Commun. 2023;11(1):110.
12. Jugé R, Breugnot J, Da Silva C, Bordes S, Closs B, Aouacheria A. Quantification and characterization of UVB-induced mitochondrial fragmentation in normal primary human keratinocytes. Sci Rep. 2016;6:35065.
13. Tondera D, Grandemange S, Jourdain A, et al. SLP-2 is required for stress-induced mitochondrial hyperfusion. EMBO J. 2009;28(11):1589-1600.
14. Utley A, Lipchick B, Lee KP, Nikiforov MA. Targeting multiple myeloma through the biology of long-lived plasma cells. Cancers. 2020;12(8):2117.
15. Lightman SM, Utley A, Lee KP. Survival of long-lived plasma cells (LLPC): piecing together the puzzle. Front Immunol. 2019;10:965.

Figure legends

Figure 1. Biphasic adaptive responses, bioenergetic reprogramming, and mitochondrial dynamics in LP-1 myeloma cells under chronic acidosis. A) Experimental timeline of MM cells exposed to control (*Ctrl*, pH*e* 7.4) or short-term acidosis (*S.A.*), mid-term acidosis (*M.A.*), and long-term acidosis (*L.A.,* pH*e* 6.8). Schematic created with BioRender.com. **B)** Longitudinal assessment of cellular proliferation via CCK-8 assay demonstrates a biphasic adaptive response to chronic acidotic stress. **C)** Quantification of apoptotic cell populations (left) and cell-cycle distribution (center) with corresponding Western blots of major

regulatory proteins (right). **D)** Metabolic profiling via Seahorse XF analysis of OCR (left) and ECAR (center). Right: Western blot validation of markers for glucose transport (SLC2A1), rate-limiting glycolytic steps (HK2, PFKP, PKM2), pyruvate flux (PDK1, LDH), and lipogenesis (FASN) to confirm acidity-driven metabolic remodeling. **E)** Representative transmission electron microscopy (TEM) images (left; 3,500×; scale bar: 500 nm) and quantitative morphological analysis of mitochondrial circularity, aspect ratio, roundness, and solidity (right) reveal significant structural remodeling upon long-term adaptation. Data presented as mean ± SD (N = 4 for apoptosis and cell cycle analysis; N = 3 for other quantitative assays). ACTB served as the loading control. Statistical significance was assessed by one-way ANOVA followed by Tukey's multiple comparison test. Comparisons were performed between the indicated groups or relative to the control. n.s., not significant ($p > 0.05$); *$p < 0.05$; **$p < 0.01$; ***$p < 0.001$.

Figure 2. Genome-wide transcriptional profiling and coordinated pathway modulation during progressive acidic adaptation in myeloma cells. A) Differential expression profiling using Affymetrix Human Clariom D Assay identified key functional gene sets and canonical pathways significantly altered under acidotic stress. The table details the normalized enrichment score (NES), *p*-values, and false discovery rates (FDR) for pairwise comparisons between control (*Ctrl*), short-term acidosis (*S.A.*), and long-term acidosis (*L.A.*). **B)** Dot plot visualization of pathway enrichment. The x-axis indicates NES, dot color represents significance ($-\log_{10}$ scale, *p*-value), size denotes the number of core genes, and shape indicates the specific comparison group. **C)** Heatmaps of leading-edge genes within significantly modulated Hallmark and Canonical gene sets. Color scale indicates the row Z-score, illustrating the transcriptional transition from an acute stress response (*S.A.*) to a

stable adaptive state (*L.A.*).

Figure 3. Genome-wide identification and clinical relevance of the acidotic adaptive signature in multiple myeloma. A) Venn diagram of differentially expressed probes across control (*Ctrl*), short-term (*S.A.*), and long-term (*L.A.*) acidic pH*e* conditions. The 178-probe intersection represents a core set consistently altered during the adaptation process. **B, C)** Heatmaps of representative upregulated and downregulated genes from the 178-probe core set that correlate with poorer overall survival in MM patients. These acid-adaptation markers are prominently involved in metabolic/mitochondrial function, cell cycle regulation and pro-apoptotic and immune-modulatory pathways; data are shown as row Z-scores. **D, E)** Clinical validation of the acidity-adaptive gene signature using the MMRF-CoMMpass dataset. Left panels: Kaplan–Meier curves (log-rank test) for the individual 7 long-term acidity-upregulated genes and 4 long-term acidity-downregulated genes. Middle panels: Kaplan–Meier curves based on the mean expression of the respective up- and downregulated gene sets, demonstrating highly significant risk stratification. Right panels: Box plots show progressive dysregulation of these gene set means across MM stages I–III (median/IQR shown; whiskers indicate min/max). Statistical significance: one-way ANOVA with Tukey's post-hoc test (**$p < 0.01$; ***$p < 0.001$). **F)** Co-expression landscape of the 11-gene core signature. Heatmap depicting the Pearson correlation coefficients among the signature genes in the MMRF-CoMMpass dataset. Red and blue shading indicates positive and negative correlations, respectively. The coherent expression pattern demonstrates the internal consistency of the signature as a coordinated molecular module.

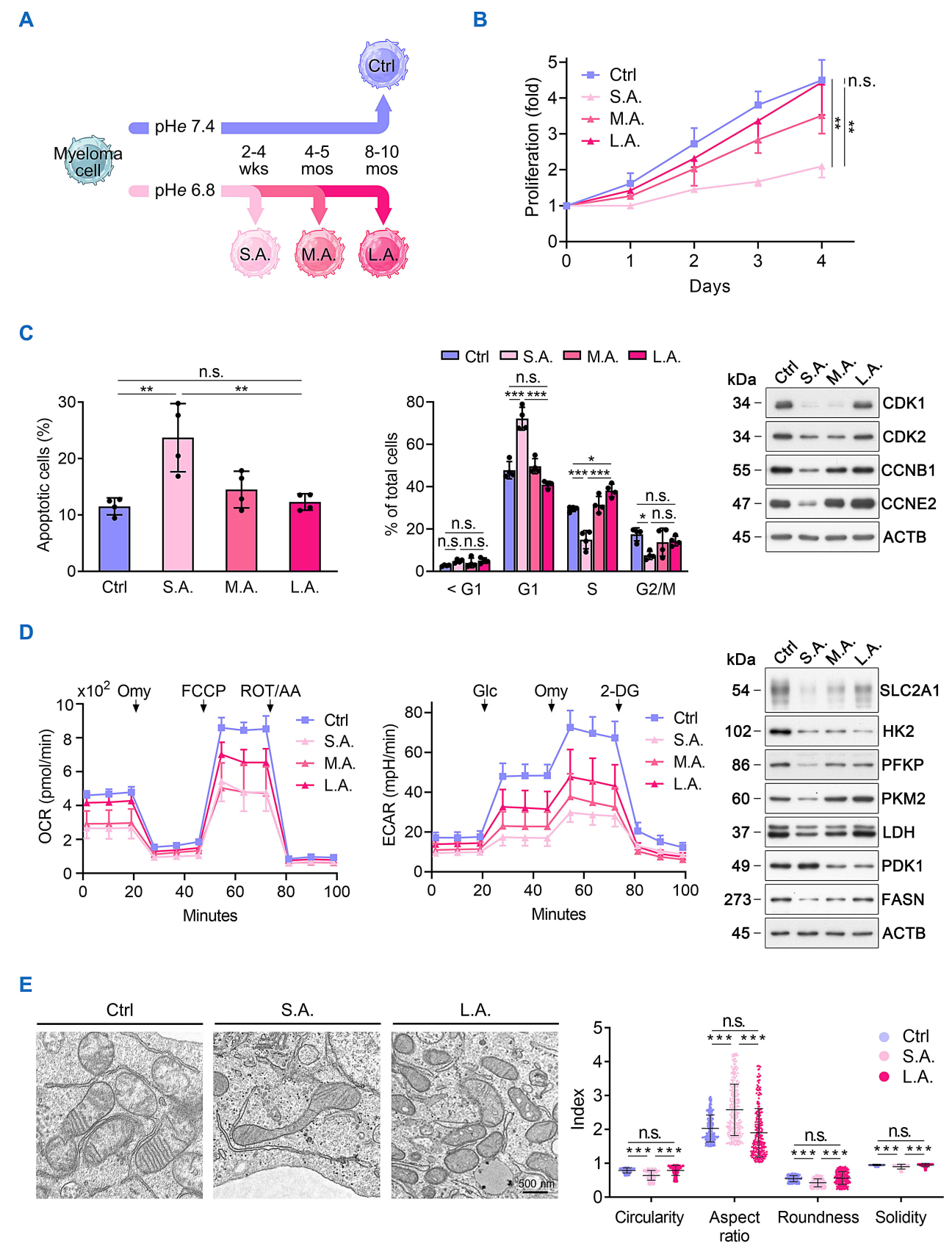
A
Ctrl
pHe 7.4
Myeloma cell
2-4 wks
4-5 mos
8-10 mos
pHe 6.8
S.A.
M.A.
L.A.
B
Proliferation (fold)
Ctrl
S.A.
M.A.
L.A.
n.s.
**
**
Days
C
Apoptotic cells (%)
n.s.
**
**
Ctrl
S.A.
M.A.
L.A.
% of total cells
< G1
G1
S
G2/M
kDa
CDK1
CDK2
CCNB1
CCNE2
ACTB
D
x10^2
Omy
FCCP
ROT/AA
OCR (pmol/min)
Minutes
Glc
Omy
2-DG
ECAR (mpH/min)
SLC2A1
HK2
PFKP
PKM2
LDH
PDK1
FASN
ACTB
E
Ctrl
S.A.
L.A.
500 nm
Index
Circularity
Aspect ratio
Roundness
Solidity

A

Hallmark Gene Sets	L.A. vs Ctrl			S.A. vs Ctrl			L.A. vs S.A.		
	NES	*p*-value	FDR	NES	*p*-value	FDR	NES	*p*-value	FDR
TGF_Beta_Signaling	2.200	<0.001	<0.001	-1.072	0.347	0.318	1.901	<0.001	0.001
E2F_Targets	1.797	<0.001	0.009	-3.277	<0.001	<0.001	3.249	<0.001	<0.001
IL6_JAK_Stat3_Signaling	1.761	<0.001	0.007	-1.201	0.151	0.154	1.584	0.008	0.013
Apoptosis	1.661	0.002	0.015	1.520	0.003	0.040	1.357	0.041	0.073
G2M_Checkpoint	1.465	0.007	0.047	-3.146	<0.001	<0.001	3.007	<0.001	<0.001

Canonical Pathways	L.A. vs Ctrl			S.A. vs Ctrl			L.A. vs S.A.		
	NES	*p*-value	FDR	NES	*p*-value	FDR	NES	*p*-value	FDR
Reactome_Meiosis	1.753	<0.001	0.186	-2.179	<0.001	<0.001	2.379	<0.001	<0.001
Reactome_DNA_Strand_Elongation	1.740	0.006	0.193	-2.581	<0.001	<0.001	2.697	<0.001	<0.001
Cell_Cycle	1.712	<0.001	0.216	-2.676	<0.001	<0.001	2.743	<0.001	<0.001
Medicus_Reference_Mismatch_Repair	1.674	0.010	0.233	-2.230	<0.001	<0.001	2.390	<0.001	<0.001

B

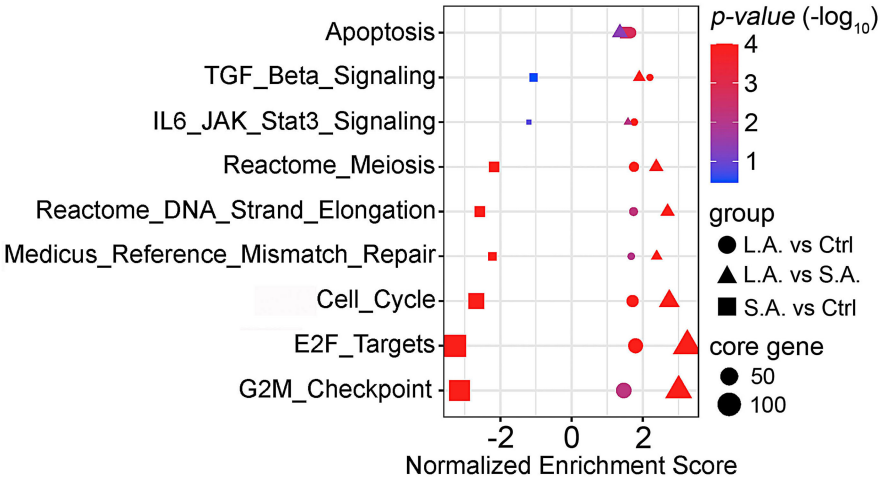

C

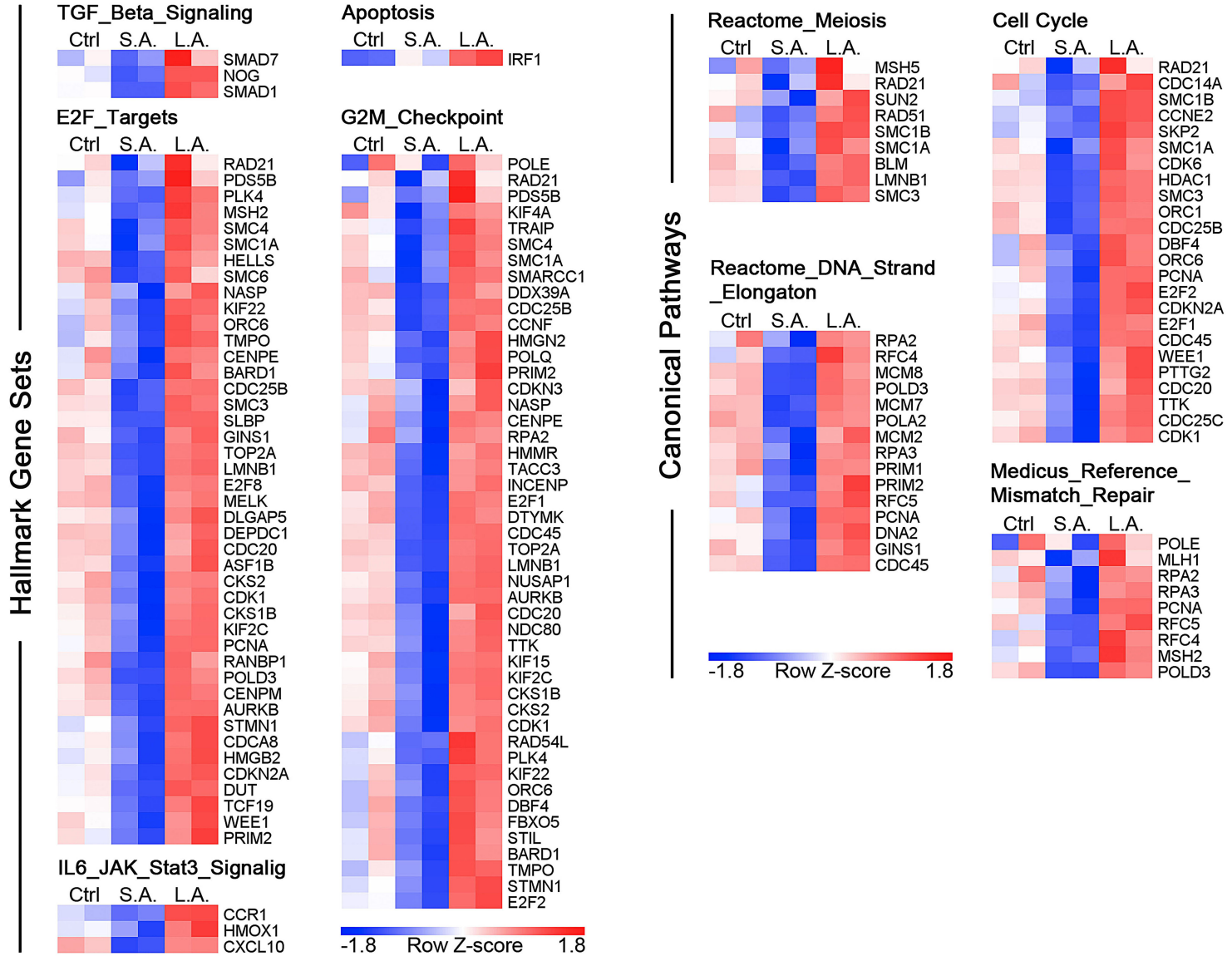

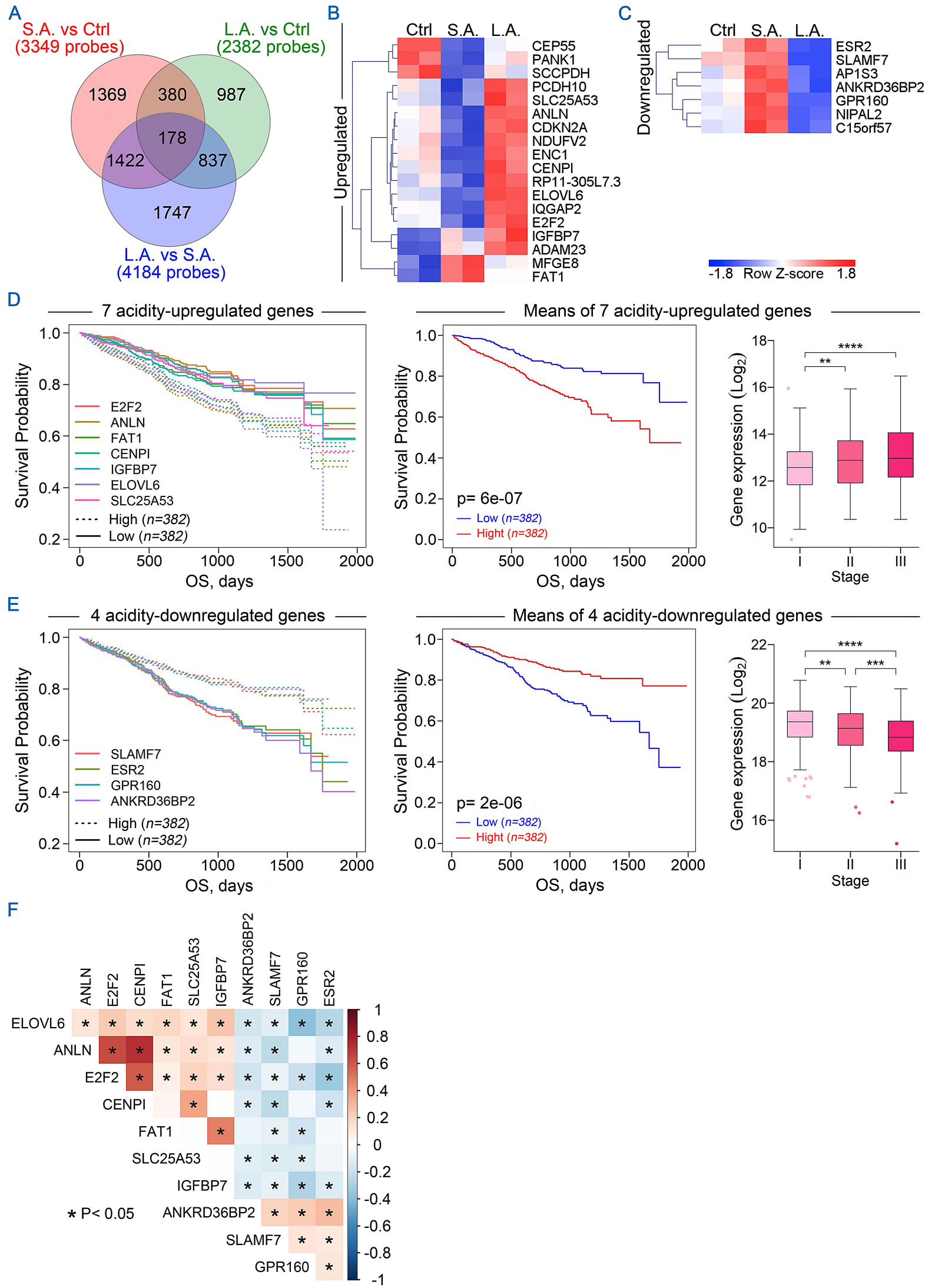
A
S.A. vs Ctrl
(3349 probes)
L.A. vs Ctrl
(2382 probes)
L.A. vs S.A.
(4184 probes)
1369
380
987
178
1422
837
1747
B
Ctrl
S.A.
L.A.
Upregulated
CEP55
PANK1
SCCPDH
PCDH10
SLC25A53
ANLN
CDKN2A
NDUFV2
ENC1
CENPI
RP11-305L7.3
ELOVL6
IQGAP2
E2F2
IGFBP7
ADAM23
MFGE8
FAT1
C
Ctrl
S.A.
L.A.
Downregulated
ESR2
SLAMF7
AP1S3
ANKRD36BP2
GPR160
NIPAL2
C15orf57
-1.8 Row Z-score 1.8
D
7 acidity-upregulated genes
Survival Probability
E2F2
ANLN
FAT1
CENPI
IGFBP7
ELOVL6
SLC25A53
High (n=382)
Low (n=382)
OS, days
Means of 7 acidity-upregulated genes
p= 6e-07
Low (n=382)
Hight (n=382)
Gene expression (Log2)
Stage
E
4 acidity-downregulated genes
SLAMF7
ESR2
GPR160
ANKRD36BP2
p= 2e-06
F
ANLN
E2F2
CENPI
FAT1
SLC25A53
IGFBP7
ANKRD36BP2
SLAMF7
GPR160
ESR2
ELOVL6
* P< 0.05

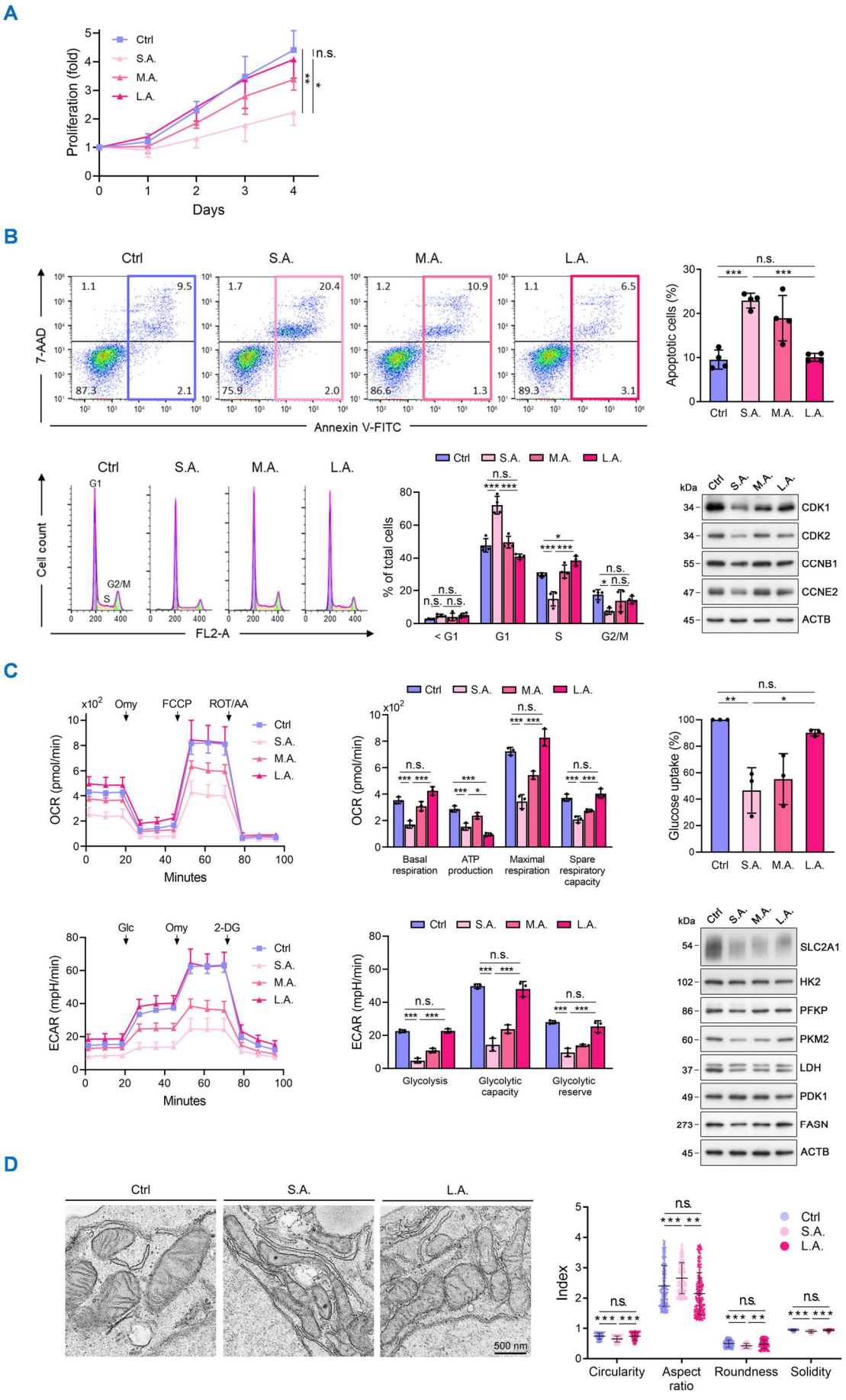

Supplementary Figure S1. Chronic acidotic stress induces biphasic adaptation, bioenergetic shifts, and mitochondrial structural changes in NCI-H929 myeloma cells. A) CCK-8 proliferation profiles demonstrating characteristic adaptive growth curves under control (*Ctrl*, pH*e* 7.4) or short-term acidosis

(*S.A.*), mid-term acidosis (*M.A.*), and long-term acidosis (*L.A.*, pH*e* 6.8). **B)** Analysis of cell death and cycle progression. Top: Representative Annexin V/7-AAD flow cytometry plots (left) and quantification of apoptotic cell populations (right). Bottom: Cell cycle distribution profiles (left), quantification of cycle phases (center), and Western blots of regulatory proteins (right) indicating recovery after initial acidotic stress. **C)** Seahorse XF metabolic analysis showing OCR and ECAR profiles (left) with quantified bioenergetic parameters (center). Accompanying panels show glucose uptake and immunoblots of glucose transporter (SLC2A1), glycolytic enzymes (HK2, PFKP, PKM2, LDH), and metabolic regulators (PDK1, FASN) to illustrate molecular shifts across different acidosis durations; ACTB served as the loading control (right). **D)** Representative TEM imagery (5,000×; scale bar: 500 nm) and mitochondrial morphological quantification (circularity, aspect ratio, roundness, and solidity) in control or acid-treated cells. Data are presented as mean ± SD (N = 3 for proliferation and metabolic assays; N = 4 for cell death and cycle analysis). Statistical significance was determined by one-way ANOVA followed by Tukey's multiple comparison test. Comparisons were performed between the indicated groups or relative to the control. n.s., not significant ($p > 0.05$); *$p < 0.05$; **$p < 0.01$; ***$p < 0.001$.

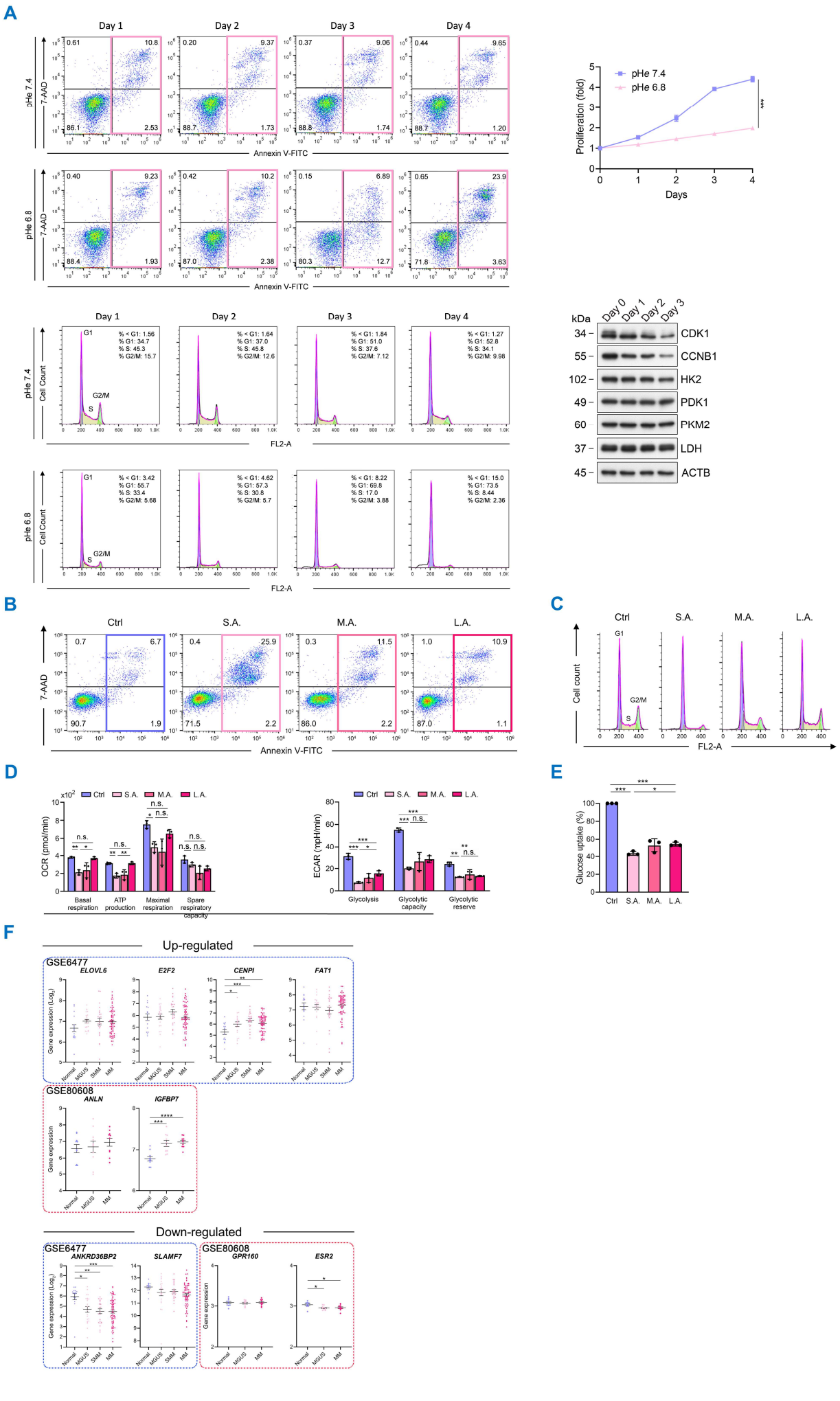
A
Day 1
Day 2
Day 3
Day 4
pHe 7.4
pHe 6.8
7-AAD
Annexin V-FITC
0.61
10.8
86.1
2.53
0.20
9.37
88.7
1.73
0.37
9.06
88.8
1.74
0.44
9.65
88.7
1.20
0.40
9.23
88.4
1.93
0.42
10.2
87.0
2.38
0.15
6.89
80.3
12.7
0.65
23.9
71.8
3.63
pHe 7.4
pHe 6.8
Proliferation (fold)
Days
***
Cell Count
FL2-A
G1
G2/M
S
% < G1: 1.56
% G1: 34.7
% S: 45.3
% G2/M: 15.7
% < G1: 1.64
% G1: 37.0
% S: 45.8
% G2/M: 12.6
% < G1: 1.84
% G1: 51.0
% S: 37.6
% G2/M: 7.12
% < G1: 1.27
% G1: 52.8
% S: 34.1
% G2/M: 9.98
% < G1: 3.42
% G1: 55.7
% S: 33.4
% G2/M: 5.68
% < G1: 4.62
% G1: 57.3
% S: 30.8
% G2/M: 5.7
% < G1: 8.22
% G1: 69.8
% S: 17.0
% G2/M: 3.88
% < G1: 15.0
% G1: 73.5
% S: 8.44
% G2/M: 2.36
kDa
Day 0
Day 1
Day 2
Day 3
34
CDK1
55
CCNB1
102
HK2
49
PDK1
60
PKM2
37
LDH
45
ACTB
B
Ctrl
S.A.
M.A.
L.A.
7-AAD
Annexin V-FITC
0.7
6.7
90.7
1.9
0.4
25.9
71.5
2.2
0.3
11.5
86.0
2.2
1.0
10.9
87.0
1.1
C
Ctrl
S.A.
M.A.
L.A.
Cell count
G1
G2/M
S
FL2-A
D
x10²
OCR (pmol/min)
Basal respiration
ATP production
Maximal respiration
Spare respiratory capacity
ECAR (mpH/min)
Glycolysis
Glycolytic capacity
Glycolytic reserve
n.s.
E
Glucose uptake (%)
F
Up-regulated
GSE6477
ELOVL6
E2F2
CENPI
FAT1
GSE80608
ANLN
IGFBP7
Gene expression (Log2)
Gene expression
Normal
MGUS
SMM
MM
Down-regulated
GSE6477
ANKRD36BP2
SLAMF7
GSE80608
GPR160
ESR2

Supplementary Figure S2. Biphasic response to acidotic stress: from acute cellular crisis and proliferative inhibition to sustained metabolic plasticity and clinical relevance. A) Acute stress response and growth suppression of LP-1 myeloma cells during initial acidic exposure (Day 1–4). (Top Left) Representative Annexin V/7-AAD flow cytometry plots showing stable viability through Day 2 under both conditions, followed by a surge in apoptosis at pH*e* 6.8 by Day 4. (Top Right) Proliferation kinetics comparing pH*e* 7.4 and pH*e* 6.8 groups over the initial 96-hour window. Statistical significance was determined by unpaired *t* test. ***$p < 0.001$. (Bottom Left) Cell cycle histograms indicating progressive G1-phase arrest with a concurrent reduction in the S and G2/M populations over 96 hours. (Bottom Right) Immunoblots of cell cycle (CDK1, CCNB1) and metabolic (HK2, PDK1, PKM2, LDH) markers illustrating the immediate molecular response to acute acidotic stress. ACTB served as the loading control. **B-C)** Longitudinal assessment of cellular kinetics. Representative flow cytometric plots for Annexin V/7-AAD staining and cell-cycle distribution in LP-1 cells under control (*Ctrl*) or acidotic stress (*S.A.*, *M.A.*, and *L.A.*) conditions over time. **D)** Quantified bioenergetic parameters from Seahorse XF analysis including respiratory (left) and glycolytic (right) metrics. **E)** Relative glucose uptake percentages confirming metabolic shifts during the transition from acute acidotic stress to stable adaptation. **F)** Clinical validation of the identified acid-adaptive gene signature. Progressive expression trajectories of the signature biomarkers across MM disease evolution using the datasets GSE6477 (130 samples; normal control, n = 15; MGUS, n = 22; SMM, n = 24; newly diagnosed MM, n = 69) and GSE80608 (30 samples; normal control, n = 10; MGUS, n = 10; MM, n = 10). An overall consistent pattern is apparent, wherein the majority of long-term acidity-upregulated genes exhibit a progressive upward trajectory, with statistically significant elevations validated in key markers in overt MM compared to normal or premalignant stages. Conversely, long-term acidity-downregulated markers generally display a reciprocal decline across progressive disease stages. Data are presented as mean ± SD. Statistical significance was determined by one-way ANOVA followed by Tukey's multiple comparison test. Comparisons were performed between the indicated groups or relative to the control. n.s., not significant ($p > 0.05$); *$p < 0.05$; **$p < 0.01$; ***$p < 0.001$.

Supplementary Table S1. Identification of the core 106-gene transcriptional signature associated with long-term adaptation of multiple myeloma cells to chronic extracellular acidosis.

A) Significantly upregulated protein-coding probes (n = 116). This table is derived from the common core subset of 178 probes that were consistently altered across the three LP-1 cell-state comparisons (*L.A.* vs *Ctrl*; *S.A.* vs *Ctrl;* and *L.A.* vs *S.A.*; see Figure 3A). It lists a total of 56 protein coding genes (116 probes) that are significantly upregulated in the long-term acidic group (*L.A.*, pH*e* 6.8) compared with the control group (*Ctrl*, pH*e* 7.4), defined by log2 fold change ≥ 1 and *p* value < 0.05. These transcripts represent the upregulated component of the core transcriptional signature underlying chronic acid adaptation in MM cells. Note: The taxon name field is left blank when no name was available. OS.*p* indicates the statistical significance of overall survival association determined by Cox proportional hazards regression analysis.

ID	Gene Symbol	Description	Log_2FC	*p*-value	OS.*p*
TC0500013316.hg.1	CD180	CD180 molecule	9.530	2.45E-07	9.24E-01
TC0200016752.hg.1	TTN	Titin	6.983	1.83E-06	1.43E-01
TC1200007626.hg.1	METTL7A	Methyltransferase like 7A	6.192	1.18E-07	5.76E-02
TC0300010943.hg.1	CCR1	Chemokine (C-C motif) receptor 1	5.756	1.86E-06	7.22E-01
TC0200007804.hg.1	AC008074.4	Novel transcript	4.215	5.36E-07	6.54E-02
TC0X00010186.hg.1			4.202	2.53E-05	
TC1200011711.hg.1	GNPTAB	N-acetylglucosamine-1-phosphate transferase alpha and beta subunits	3.794	2.90E-05	3.53E-02
TC0200006627.hg.1	ID2	Inhibitor of DNA binding 2	3.741	1.10E-05	1.35E-01
TC0100009241.hg.1	S1PR1	Sphingosine-1-phosphate receptor 1	3.548	2.48E-04	9.31E-02
TC1500010422.hg.1	IDH2	Isocitrate dehydrogenase 2 (NADP+)	3.477	1.48E-05	9.08E-02
TC1000008413.hg.1	AL139340.1		3.126	1.30E-05	7.28E-01
TC1200006843.hg.1	AC078950.1		3.126	1.30E-05	8.58E-01
TC1100011778.hg.1	AP002802.1		3.121	8.55E-06	9.94E-01
TC0500012113.hg.1	mawoby	Transcript Identified by AceView	3.115	3.77E-04	
TC0400010785.hg.1	IGFBP7	Insulin like growth factor binding protein 7	3.057	4.71E-04	3.11E-03
TC0700009668.hg.1	ZBED6CL	ZBED6 C-terminal like	2.976	8.09E-06	9.57E-01
TC0900007720.hg.1	AL133391.1		2.952	3.80E-05	5.71E-01
TC0X00008620.hg.1	AL109620.1		2.952	3.80E-05	1.10E-01
TC1000011112.hg.1	AC013738.1		2.951	9.92E-06	9.93E-01
TC0700011079.hg.1	AC006478.1		2.924	1.28E-05	1.14E-01
TC2100006982.hg.1	LINC00649	Long intergenic non-protein coding RNA 649	2.881	1.31E-05	1.96E-01
TC1200010559.hg.1	VDR	Vitamin D receptor	2.761	8.18E-06	5.28E-03
TC1200010794.hg.1	ITGB7	Integrin beta 7	2.723	9.54E-06	5.06E-02
TC0400012956.hg.1	ELOVL6	ELOVL fatty acid elongase 6	2.715	1.30E-05	2.15E-04
TC0900011421.hg.1	AL365274.1		2.694	1.64E-05	5.74E-01
TC1800008925.hg.1	AC027506.1		2.694	1.64E-05	2.58E-01
TC2000007083.hg.1	ID1	Inhibitor of DNA binding 1	2.527	3.86E-05	9.78E-02
TC0200010371.hg.1	foswaby	Transcript Identified by AceView	2.424	1.78E-03	

TC1700008350.hg.1	NOG	Noggin	2.348	7.74E-05	3.39E-01
TC0400012947.hg.1	GPRIN3	GPRIN family member 3	2.345	3.57E-03	3.55E-01
TC0200010577.hg.1	ADAM23	ADAM metallopeptidase domain 23	2.329	5.70E-05	3.06E-06
TC0300007351.hg.1	AC141002.1		2.311	8.87E-05	3.72E-01
TC0900012154.hg.1	TMEFF1	Transmembrane protein with EGF-like and two follistatin-like domains 1	2.276	9.57E-05	1.67E-01
TC0900012155.hg.1	MSANTD3-TMEFF1	MSANTD3-TMEFF1 readthrough	2.266	1.04E-04	7.86E-01
TC0600009291.hg.1			2.256	7.80E-05	
TC0X00010434.hg.1	SLC25A53	Solute carrier family 25 member 53	2.248	1.56E-03	1.99E-03
TC0100017110.hg.1	FCMR	Fc fragment of IgM receptor	2.233	9.11E-04	
TC0700010965.hg.1	IGFBP3	Insulin like growth factor binding protein 3	2.169	9.75E-05	1.31E-01
TC0300008316.hg.1	PVRL3	Poliovirus receptor-related 3	2.114	1.39E-03	6.26E-01
TC0400012938.hg.1	RASGEF1B	RasGEF domain family member 1B	2.085	3.85E-04	6.01E-01
TC0200010370.hg.1			2.085	2.87E-04	
TC2200006436.hg.1			2.069	6.05E-04	
TC0300012872.hg.1			2.068	2.34E-04	
TC0300012531.hg.1			2.058	1.02E-04	
TC0500008483.hg.1	SNX24	Sorting nexin 24	2.057	1.12E-04	1.51E-02
TC0400008725.hg.1	PCDH10	Protocadherin 10	2.028	5.39E-03	1.31E-03
TC0900010535.hg.1	AL354682.1		2.027	5.56E-05	9.01E-01
TC0900008238.hg.1	MURC	Muscle-related coiled-coil protein	1.992	4.32E-04	2.52E-01
TC0700010281.hg.1	THSD7A	Thrombospondin type 1 domain containing 7A	1.962	1.50E-03	3.07E-01
TC1100012840.hg.1			1.937	9.72E-05	
TC0900007715.hg.1	LOC105376111	Uncharacterized LOC105376111	1.896	2.13E-03	
TC0500007770.hg.1	FOXD1-AS1	FOXD1 antisense RNA 1	1.888	3.28E-03	
TC0300006466.hg.1			1.885	9.42E-05	
TC0100015866.hg.1	S100A4	S100 calcium binding protein A4	1.849	9.50E-03	2.88E-01
TC0400012670.hg.1	FAT1	FAT atypical cadherin 1	1.831	1.07E-03	2.40E-03
TC0800007362.hg.1	PLEKHA2	Pleckstrin homology domain containing family A member 2	1.824	1.20E-04	1.67E-01
TC1600010951.hg.1	MAF	V-maf avian musculoaponeurotic fibrosarcoma oncogene homolog	1.801	2.18E-04	9.73E-01
TC0900009813.hg.1	AL353783.1		1.790	2.90E-04	6.90E-01
TC0X00010761.hg.1	AL596243.1		1.790	2.90E-04	4.09E-01
TC0100013289.hg.1	flawlarbo	Transcript Identified by AceView	1.781	2.12E-03	
TC1100009849.hg.1	plargler	Transcript Identified by AceView	1.766	9.67E-04	
TC0300008319.hg.1			1.759	9.11E-04	
TC1700006655.hg.1	ENO3	Enolase 3	1.754	4.61E-03	1.26E-01
TC0800010894.hg.1	HEY1	Hes-related family bHLH transcription factor with YRPW motif 1	1.713	5.55E-03	1.49E-01
TC0400011487.hg.1			1.691	5.08E-04	
TC0400007147.hg.1			1.679	5.05E-04	

TC0200006725.hg.1	GREB1	Growth regulation by estrogen in breast cancer 1	1.677	1.70E-04	7.55E-02
TC0700008070.hg.1	starsmawbu	Transcript Identified by AceView	1.620	1.15E-02	
TC0800011370.hg.1			1.575	1.58E-02	
TC1100007899.hg.1	RARRES3	Retinoic acid receptor responder 3	1.574	9.68E-04	3.38E-01
TC1400010433.hg.1			1.543	1.25E-02	
TC0100010672.hg.1	RABGAP1L	RAB GTPase activating protein 1-like	1.539	1.94E-03	7.56E-01
TC1800006632.hg.1	RP11-888D10.4	Novel transcript, sense intronic to ANKRD12	1.536	8.28E-03	7.28E-01
TC0900006865.hg.1	snerplubu	Transcript Identified by AceView	1.505	7.44E-04	
TC1200006995.hg.1	pleyblybu	Transcript Identified by AceView	1.473	7.81E-03	
TC0400011578.hg.1	CASP6	Caspase 6	1.456	1.33E-03	2.62E-01
TC0800009512.hg.1	plybla	Transcript Identified by AceView	1.449	4.12E-04	
TC0500007826.hg.1	IQGAP2	IQ motif containing GTPase activating protein 2	1.449	4.30E-04	2.34E-02
TC0200014597.hg.1	RND3	Rho family GTPase 3	1.443	2.50E-02	1.31E-01
TC0900010758.hg.1	RP11-305L7.3	Novel transcript	1.432	3.85E-03	1.82E-04
TC0400011725.hg.1			1.429	1.51E-03	
TC1300007351.hg.1	gleeshorbu	Transcript Identified by AceView	1.413	8.16E-03	
TC0500009211.hg.1	CYFIP2	Cytoplasmic FMR1 interacting protein 2	1.408	8.65E-04	1.25E-01
TC1100007394.hg.1	CD82	CD82 molecule	1.404	6.60E-04	8.96E-01
TC0X00010512.hg.1	CHRDL1	Chordin-like 1	1.376	8.80E-03	9.03E-02
TC1000006995.hg.1	COMMD3-BMI1	COMMD3-BMI1 readthrough	1.342	1.91E-03	2.82E-01
TC0900012219.hg.1	CDKN2A	Cyclin-dependent kinase inhibitor 2A	1.318	3.16E-03	6.89E-03
TC1500010369.hg.1	MFGE8	Milk fat globule-EGF factor 8 protein	1.297	7.97E-03	3.03E-02
TC1100006929.hg.1	blargloy	Transcript Identified by AceView	1.274	6.33E-03	
TC0700007198.hg.1	ANLN	Anillin actin binding protein	1.265	1.74E-03	5.72E-06
TC0100013287.hg.1	E2F2	E2F transcription factor 2	1.240	2.87E-03	2.04E-07
TC0500011146.hg.1	ENC1	Ectodermal-neural cortex 1	1.237	4.14E-03	3.35E-04
TC0X00007936.hg.1	CENPI	Centromere protein I	1.235	6.05E-03	7.77E-09
TC1000008646.hg.1	OLMALINC	Oligodendrocyte maturation-associated long intergenic non-coding RNA	1.232	1.87E-02	2.78E-01
TC0300011655.hg.1	jorspaby	Transcript Identified by AceView	1.224	2.22E-02	
TC0800012457.hg.1	TMEM65	transmembrane protein 65	1.219	5.96E-03	7.57E-01
TC0300006465.hg.1	LRRN1	Leucine rich repeat neuronal 1	1.206	2.08E-03	2.84E-01
TC0100010543.hg.1	ATP1B1	ATPase Na+/K+ transporting beta 1 polypeptide	1.201	1.28E-03	1.12E-01
TC1100010383.hg.1			1.155	3.08E-03	
TC1100011050.hg.1	FADS1	Fatty acid desaturase 1	1.153	2.88E-03	1.00E-01
TC2200007496.hg.1	jeybar	Transcript Identified by AceView	1.146	1.75E-02	
TC0200012230.hg.1	AC073218.3	Putative novel transcript	1.126	2.21E-02	5.41E-01
TC1800006841.hg.1	MIB1	Mindbomb E3 ubiquitin protein ligase 1	1.125	2.85E-03	9.65E-02
TC0500013266.hg.1	HMP19	HMP19 protein	1.106	7.16E-03	5.22E-01

TC2200009274.hg.1	APOBEC3G	Apolipoprotein B mRNA editing enzyme catalytic polypeptide-like 3G	1.099	6.43E-03	4.30E-01
TC0700008729.hg.1	wyflubu	Transcript Identified by AceView	1.076	6.89E-03	
TC0100016386.hg.1	RP1-45C12.1	Novel transcript, antisense to FMO1	1.074	5.98E-03	7.81E-01
TC0300011654.hg.1	chordybo	Transcript Identified by AceView	1.070	2.36E-02	
TC0700007034.hg.1	CREB5	cAMP responsive element binding protein 5	1.062	4.70E-02	4.12E-01
TC0300009258.hg.1	MME	Membrane metallo-endopeptidase	1.060	8.58E-03	1.61E-01
TC1200008425.hg.1	RP11-796E2.4	Novel transcript, antisense to BTG1	1.047	1.90E-02	9.89E-02
TC0100014617.hg.1	SLC44A5	Solute carrier family 44 member 5	1.041	8.27E-03	2.80E-01
TC1800009214.hg.1	NDUFV2	NADH dehydrogenase (ubiquinone) flavoprotein 2	1.032	1.09E-02	5.36E-03
TC1100012165.hg.1	CASP4	Caspase 4	1.032	2.78E-03	2.27E-02
TC0200016222.hg.1	HES6	Hes family bHLH transcription factor 6	1.021	6.63E-03	1.11E-01
TC1100010387.hg.1			1.001	4.30E-02	

B) Significantly downregulated protein-coding probes (n = 62). This table is derived from the common core subset of 178 probes that were consistently altered across the three LP-1 cell-state comparisons (*L.A.* vs *Ctrl*; *S.A.* vs *Ctrl*; and *L.A.* vs *S.A.*; see Figure 3A). It lists a total of 50 protein coding genes (62 probes) that are significantly downregulated in the long-term acidic group (*L.A.*, pH*e* 6.8) compared with the control group (*Ctrl*, pH*e* 7.4), defined by log2 fold change ≤ -1 and *p* value < 0.05. These transcripts represent the downregulated component of the core transcriptional signature underlying chronic acid adaptation in MM cells. Note: The taxon name field is left blank when no name was available. OS.*p* indicates the statistical significance of overall survival association determined by Cox proportional hazards regression analysis.

ID	Gene Symbol	Description	Log_2FC	*P*-value	OS.*p*
TC0100010310.hg.1	SLAMF7	SLAM family member 7	-7.151	2.60E-08	3.42E-04
TC1200007881.hg.1	INHBE	Inhibin beta E	-4.126	9.44E-07	6.40E-02
TC0100015822.hg.1	S100A11	S100 calcium binding protein A11	-3.309	2.66E-04	7.66E-01
TC0700012443.hg.1	FEZF1	FEZ family zinc finger 1	-3.006	5.09E-05	1.09E-01
TC1200011914.hg.1	HVCN1	Hydrogen voltage gated channel 1	-2.619	1.07E-04	5.35E-01
TC0200008099.hg.1	HK2	Hexokinase 2	-2.585	9.37E-05	1.06E-01
TC1000009893.hg.1	ITGA8	Integrin alpha 8	-2.404	3.35E-04	7.81E-01
TC0200008353.hg.1	ANKRD36BP2	Ankyrin repeat domain 36B pseudogene 2	-2.399	4.09E-04	2.59E-03
TC0800011211.hg.1	NIPAL2	NIPA-like domain containing 2	-2.216	5.68E-05	1.73E-02
TC1400009402.hg.1	ESR2	Estrogen receptor 2 (ER beta)	-2.198	4.80E-04	2.99E-02
TC0400011732.hg.1	NDNF	Neuron-derived neurotrophic factor	-2.173	4.83E-04	9.30E-01
TC1800007014.hg.1	DSG2	Desmoglein 2	-2.162	1.84E-04	2.62E-02
TC0700008745.hg.1	PRKAR2B	Protein kinase cAMP-dependent regulatory type II beta	-2.155	6.54E-04	3.75E-01
TC0300009459.hg.1	GPR160	G protein-coupled receptor 160	-2.149	4.41E-04	8.59E-03
TC0800008801.hg.1	TRIB1	Tribbles pseudokinase 1	-2.004	9.63E-05	6.24E-01
TC0100015397.hg.1	CD58	CD58 molecule	-1.950	1.89E-03	1.07E-01
TC1300010032.hg.1	SOHLH2	Spermatogenesis and oogenesis specific basic helix-loop-helix 2	-1.934	1.47E-03	7.12E-01
TC1800007326.hg.1	ME2	Malic enzyme 2	-1.893	1.05E-04	7.79E-02
TC1000008482.hg.1	CEP55	Centrosomal protein 55kDa	-1.810	1.81E-04	1.33E-06

TC1500008442.hg.1	NR2F2	Nuclear receptor subfamily 2 group F member 2	-1.794	1.21E-04	2.63E-01
TC1800006706.hg.1	GNAL	Guanine nucleotide binding protein (G protein)	-1.715	1.62E-04	9.30E-01
TC0600011773.hg.1	TREML2	Triggering receptor expressed on myeloid cells-like 2	-1.610	2.29E-04	7.43E-03
TC2200006517.hg.1	CECR2	Cat eye syndrome chromosome region, candidate 2	-1.582	4.04E-04	6.32E-01
TC1500006643.hg.1	GABRA5	Gamma-aminobutyric acid (GABA) A receptor alpha 5	-1.541	6.56E-03	1.18E-02
TC1800007440.hg.1	ZNF532	Zinc finger protein 532	-1.539	1.18E-03	7.36E-02
TC0100012278.hg.1	SCCPDH	Saccharopine dehydrogenase (putative)	-1.524	3.58E-03	1.01E-02
TC0500012870.hg.1	STC2	Stanniocalcin 2	-1.485	1.53E-03	4.35E-02
TC0X00009205.hg.1	SH3KBP1	SH3-domain kinase binding protein 1	-1.485	2.43E-03	5.63E-02
TC0200010264.hg.1	MFSD6	Major facilitator superfamily domain containing 6	-1.426	7.82E-04	5.73E-02
TC1200010145.hg.1	BCAT1	Branched chain amino-acid transaminase 1	-1.425	4.93E-04	6.10E-01
TC1700011436.hg.1	ERN1	Endoplasmic reticulum to nucleus signaling 1	-1.423	2.99E-03	7.39E-01
TC1500010886.hg.1	CALML4	Calmodulin-like 4	-1.408	7.07E-04	9.90E-01
TC1300010031.hg.1	CCDC169-SOHLH2	CCDC169-SOHLH2 readthrough	-1.375	1.39E-03	3.76E-01
TC0100008874.hg.1	PRKACB	Protein kinase cAMP-dependent catalytic beta	-1.328	6.27E-03	6.89E-01
TC0800011748.hg.1	skarwarbu	Transcript Identified by AceView	-1.328	5.87E-03	
TC0300013684.hg.1	TFRC	Transferrin receptor	-1.310	1.75E-03	7.38E-01
TC0100015350.hg.1	AMPD1	Adenosine monophosphate deaminase 1	-1.299	1.22E-03	8.66E-01
TC0100017491.hg.1	ENAH	Enabled homolog (Drosophila)	-1.294	3.68E-03	4.54E-01
TC0400011731.hg.1			-1.293	5.09E-03	
TC0400007511.hg.1	DANCR	Differentiation antagonizing non-protein coding RNA	-1.270	1.50E-03	4.02E-01
TC0500010540.hg.1	LIFR	Leukemia inhibitory factor receptor alpha	-1.263	1.07E-03	4.99E-01
TC0300012718.hg.1	PLOD2	Procollagen-lysine, 2-oxoglutarate 5-dioxygenase 2	-1.238	3.88E-03	9.71E-01
TC0600014236.hg.1	TXNDC5	Thioredoxin domain containing 5	-1.227	1.27E-03	2.15E-01
TC1000006652.hg.1	PFKFB3	6-phosphofructo-2-kinase/fructose-2,6-biphosphatase 3	-1.212	4.14E-03	8.92E-01
TC1500010723.hg.1	CHAC1	ChaC glutathione-specific gamma-glutamylcyclotransferase 1	-1.195	3.49E-03	1.10E-01
TC1000011382.hg.1	PANK1	Pantothenate kinase 1	-1.161	5.88E-03	2.46E-02
TC1500009109.hg.1	C15orf57	Chromosome 15 open reading frame 57	-1.140	4.68E-03	4.09E-03
TC0200010410.hg.1	SPATS2L	Spermatogenesis associated serine-rich 2-like	-1.134	4.86E-03	1.78E-01
TC1700010183.hg.1			-1.129	5.54E-03	
TC1800007340.hg.1	DCC	DCC netrin 1 receptor	-1.119	2.53E-03	1.56E-02
TC1700010798.hg.1	DUSP3	Dual specificity phosphatase 3	-1.115	1.01E-02	3.83E-01
TC0200013376.hg.1	EIF2AK3	Eukaryotic translation initiation factor 2-alpha kinase 3	-1.113	3.17E-03	1.62E-01
TC1800008080.hg.1			-1.097	7.49E-03	
TC0100016162.hg.1	B4GALT3	Beta 1,4- galactosyltransferase 3	-1.097	6.59E-03	8.28E-02
TC0500008309.hg.1	CAMK4	Calcium/calmodulin-dependent protein kinase IV	-1.092	3.20E-03	4.73E-01
TC0900010311.hg.1	FAM27E3	Family with sequence similarity 27 member E3	-1.090	3.47E-02	9.19E-01
TC2100007402.hg.1	ADARB1	Adenosine deaminase RNA-specific B1	-1.088	2.20E-03	2.10E-01
TC0200015869.hg.1	AP1S3	Adaptor-related protein complex 1 sigma 3 subunit	-1.051	9.33E-03	9.75E-03
TC0X00007951.hg.1	ARMCX3	Armadillo repeat containing X-linked 3	-1.050	4.77E-03	1.31E-01

TC1700007216.hg.1	CCDC144CP	Coiled-coil domain containing 144C, pseudogene	-1.020	2.97E-02	4.77E-01
TC0700013439.hg.1	BCAP29	B-cell receptor-associated protein 29	-1.010	6.11E-03	7.00E-01
TC0X00011180.hg.1	RENBP	Renin binding protein	-1.005	1.99E-02	9.54E-01